minerals

MDPI

*Article*

# Increase in Recovery Efficiency of Iron-Containing Components from Ash and Slag Material (Coal Combustion Waste) by Magnetic Separation

**Tatiana Aleksandrova [1], Nadezhda Nikolaeva [1], Anastasia Afanasova [1,*], Duan Chenlong [2], Artyem Romashev [1], Valeriya Aburova [1] and Evgeniya Prokhorova [1]**

[1] Department of Mineral Processing, Saint Petersburg Mining University, 199106 St. Petersburg, Russia; aleksandrova_tn@pers.spmi.ru (T.A.); nadegdaspb@mail.ru (N.N.); romashev_ao@pers.spmi.ru (A.R.); lera.aburova@mail.ru (V.A.); proh98jane@gmail.com (E.P.)

[2] Key Laboratory of Coal Processing and Efficient Utilization of Ministry of Education, School of Chemical Engineering and Technology, China University of Mining and Technology, Xuzhou 221116, China; clduan@cumt.edu.cn

* Correspondence: afanasova_av@pers.spmi.ru

**Abstract:** This article presents the results of research aimed at optimizing the process of recovery of valuable components from ash and slag waste from thermal power plants. In this work, both experimental and theoretical studies were carried out to substantiate the use of magnetic separation methods for ash and slag waste processing. Ash and slag wastes were chosen as an object of research due to the presence of valuable components such as iron, aluminum, etc., in them. The research results showed that the method of magnetic separation, including high-gradient magnetic separation, can be effectively used in ash and slag waste processing. As a result, the topology of a magnetic beneficiation technological scheme has been proposed to obtain high-value-added products such as high-magnetic iron minerals, low-magnetic iron minerals, and aluminosilicate microspheres. By using magnetic separation in a weak magnetic field, magnetic microspheres containing high-magnetic iron minerals associated with intermetallics, ranging in size from 20 to 80 µm, were recovered. In the second stage of magnetic separation (high-gradient magnetic separation), an iron ore product with an iron content of 50% with a recovery of 92.07% could be obtained. By using scanning electron microscopy, it was found that the main part of microspheres, which contain low-magnetic iron minerals and aluminosilicates, with sizes from 2 to 15 microns, was recovered in the magnetic fraction. This paper proposes a new approach to the enrichment of ash and slag materials using magnetic separation, which will increase the efficiency of their processing and make the process environmentally sustainable.

**Keywords:** high-gradient magnetic separation; ash and slag waste from thermal power plants; microspheres; intermetallics; iron; aluminum



**Citation:** Aleksandrova, T.; Nikolaeva, N.; Afanasova, A.; Chenlong, D.; Romashev, A.; Aburova, V.; Prokhorova, E. Increase in Recovery Efficiency of Iron-Containing Components from Ash and Slag Material (Coal Combustion Waste) by Magnetic Separation. *Minerals* **2024**, *14*, 136. https://doi.org/10.3390/min14020136

Academic Editors: Elvis Fosso-Kankeu, Pierfranco Lattanzi, Elisabetta Dore, Fabio Perlatti and Hendrik Gideon Brink

Received: 17 October 2023
Revised: 11 January 2024
Accepted: 23 January 2024
Published: 26 January 2024



## 1. Introduction

Due to the growth of the world population and its needs, the demand for electricity is increasing [1,2]. Access to both energy resources and electricity itself is a necessary condition for the growth of the world economy. The main sources of electricity can be divided into three main groups: fossil fuels (oil, gas, coal, and oil shale), nuclear and thermonuclear fusion energy, and renewable energy sources (water, wind, solar energy, etc.) [3–7]. At present, a large portion of electricity generation is provided by fossil fuels, while the portion of renewable energy sources is still insignificant [8,9]. In 2021, at the 26th UN Climate Change Conference (COP26), commitments were accepted to reduce the carbon footprint and gradually reduce the use of coal energy [10].

Currently, coal power generation is one of the largest sources of electricity in the world, accounting for 36% of global electricity generation in 2022 [11]. In the present conditions of the world economy, even considering the tendency to reduce the use of fossil fuels, coal power will retain its leading position [12]. Consequently, there is a huge number of power plants in the world that are operated by coal. At coal power plants, electricity is generated by coal combustion. Which generates a huge amount of waste (ash and slag waste) [13–15].

Under these conditions, the involvement of ash and slag wastes in economic turnover becomes a priority, which will allow us to obtain additional economic effects and reduce the environmental impact in the regions of placement [16,17]. Depending on the deposit and quality of coal, as well as the conditions of its combustion, the generated ash and slag wastes have different compositions and different physical and chemical properties [18]. The main directions of ash and slag waste processing can be highlighted as follows: production of building materials, various fill materials, and soil stabilizers; road building; recultivation of mined-out pits; as well as use as secondary raw materials for the recovery of valuable components [19,20].

Critical reviews of previous studies have shown that in ash and slag wastes, elements (Fe, Si, Ti, Al, Ni, Mo, V, and many others) are present in significant amounts, some of them being strategic metals for a number of industries [21–25]. Various beneficiation processes are used to recover these valuable components: flotation and gravity concentration [26,27], magnetic separation [28–30], and leaching processes [31–33].

Magnetic and aluminosilicate microspheres are one of the components included in ash and slag waste, which have unique technological properties, and they are of industrial interest for recovery [34]. Magnetic and flotation methods are most often used for their separation, but their efficiency is not high enough, which is due to the size of the material (most of it is in the class of 40 µm) [35]. A perspective direction for the recovery of magnetic and aluminosilicate microspheres from fine classes is the use of high-gradient magnetic separation [36–40].

Thus, the aim of this work was to determine and investigate the dependence of magnetic separation process efficiency from the technological parameters of a high-gradient magnetic separator for the recovery of valuable components in the processing of ash and slag wastes as an additional commercial product.

## 2. Materials and Methods

### *2.1. Characteristics of Research Objects*

Ash and slag waste (ASW) of coal heat power plants (CHPP) weighing 100 kg was chosen as the object of research. For all investigations, representative samples of the required mass were taken in the amount of three samples for each test. Representative samples of 500 g were taken for sieve analysis. Sieve analysis was performed to determine the particle size distribution of the sample. The sample of each size class was analyzed using a Shimadzu EDX 700 X-ray fluorescence analyzer (Shimadzu Corporation, Kyoto, Japan). The results of the analysis are presented in Table 1.

**Table 1.** Results of X-ray fluorescence analysis of size classes after sieve analysis of the sample.

| Size Class, mm | Yield, % | Content, % | | | | | | | | | | | | |
|---|---|---|---|---|---|---|---|---|---|---|---|---|---|---|
| | | Fe | Si | S | As | Al | Ca | Sb | K | Mn | Zn | Cu | Ni | Sr |
| +0.800 | 0.13 | 31.55 | 16.23 | 3.53 | 2.75 | 1.17 | 2.18 | 1.03 | 0.81 | 0.14 | 0.076 | 0.069 | 0.034 | 0.011 |
| −0.800 + 0.425 | 0.14 | 30.82 | 15.84 | 3.24 | 3.05 | 1.44 | 3.19 | 1.41 | 1.02 | 0.18 | 0.073 | 0.121 | 0.039 | 0.014 |
| −0.425 + 0.212 | 1.16 | 29.35 | 16.43 | 2.58 | 3.38 | 1.65 | 3.48 | 2.22 | 0.77 | 0.18 | 0.076 | 0.068 | 0.038 | 0.013 |
| −0.212 + 0.106 | 0.80 | 28.52 | 15.85 | 2.89 | 2.77 | 2.32 | 3.94 | 1.88 | 1.10 | 0.18 | 0.073 | 0.069 | 0.033 | 0.014 |
| −0.106 + 0.045 | 4.40 | 23.79 | 16.85 | 6.33 | 3.07 | 2.28 | 1.84 | 0.82 | 1.78 | 0.13 | 0.049 | 0.047 | 0.021 | 0.010 |
| −0.045 + 0 | 93.37 | 29.97 | 15.80 | 2.45 | 3.44 | 2.31 | 3.37 | 2.02 | 0.83 | 0.19 | 0.074 | 0.074 | 0.037 | 0.012 |
| Total | 100 | 29.68 | 15.85 | 2.63 | 3.42 | 2.30 | 3.31 | 1.97 | 0.87 | 0.19 | 0.07 | 0.073 | 0.036 | 0.012 |

As shown in Table 1, ASW has a significant yield of fine grades, with 93.37% represented in the −45 µm fraction. When beneficiating material in this size range, it is very difficult to produce a concentrate of suitable quality. Analysis of the various size grades was carried out using a Vega 3 LMH electron microscope (TESCAN, Brno, Czech Republic) equipped with an Oxford Instruments (Oxfordshire, UK) INCA Energy 250/X-max 20 energy-dispersive microanalyzer. Micrographs of the particles are shown in Figure 1.

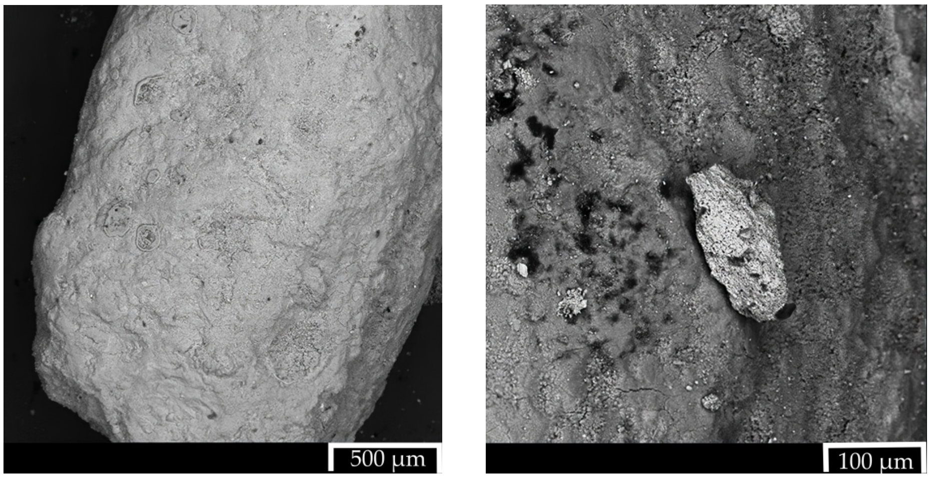


(**a**)

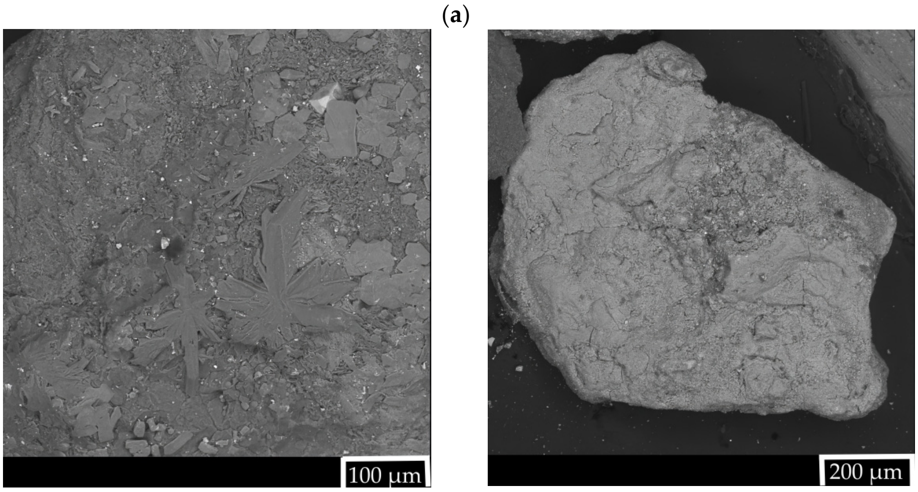


(**b**)

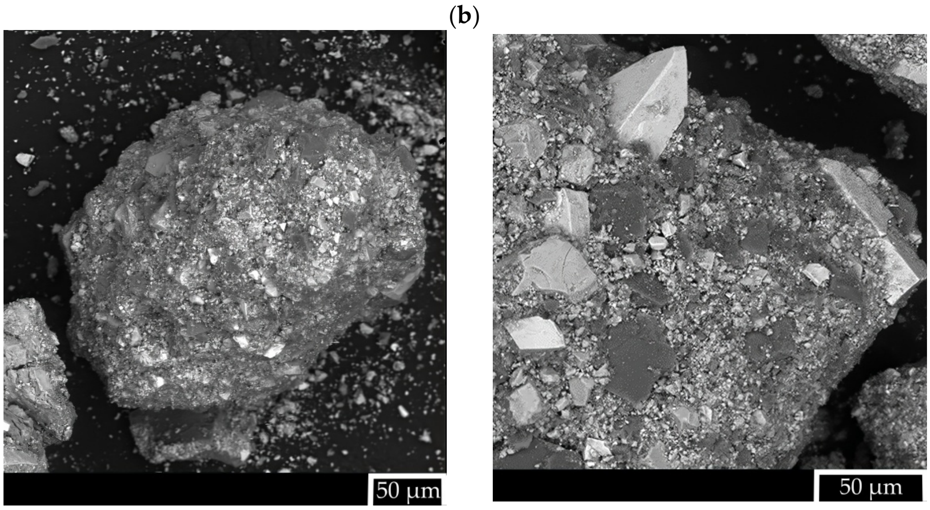


(**c**)

**Figure 1.** *Cont.*

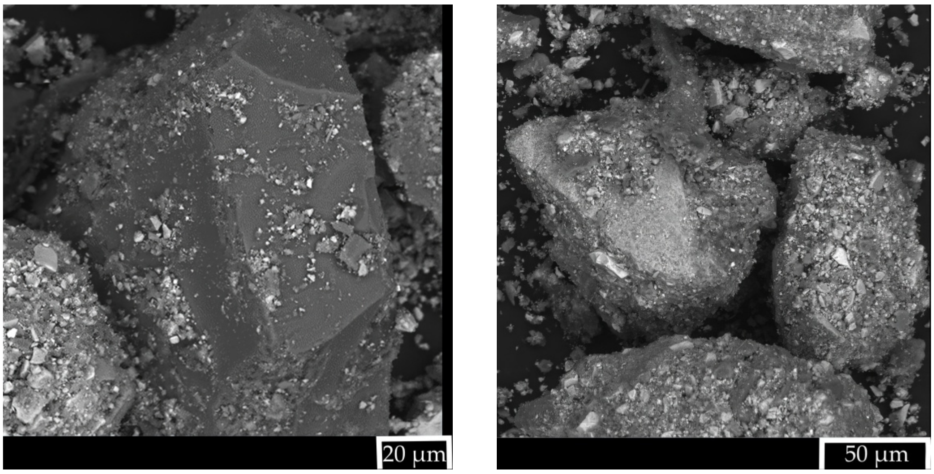


(**d**)

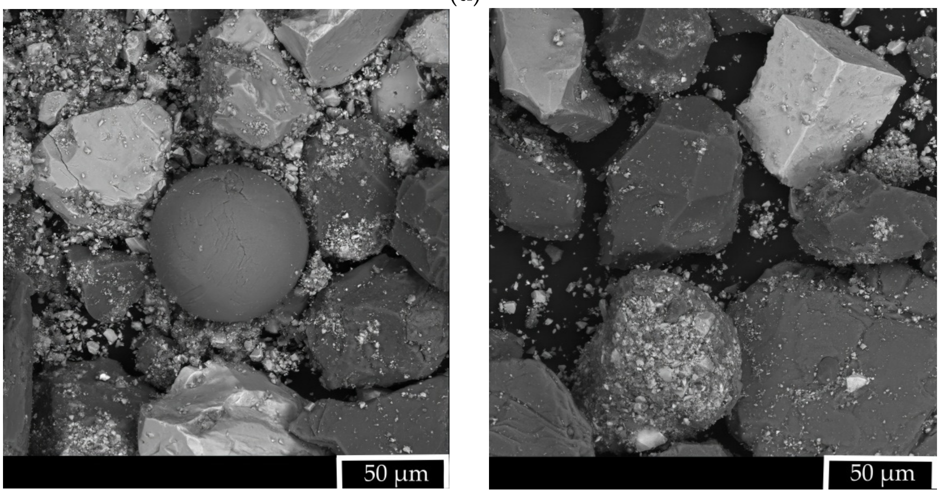


(**e**)

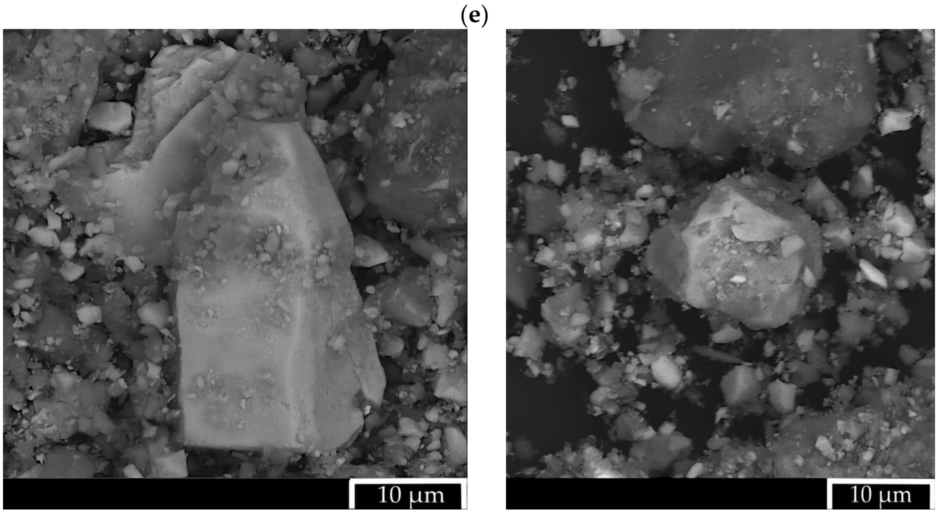


(**f**)

**Figure 1.** Microphotographs of ASW by size grade (BSE): (**a**) + 0.8 mm; (**b**) -0.8 + 0.425 mm; (**c**) −0.425 + 0.212 mm; (**d**) −0.212 + 0.106 mm; (**e**) −0.106 + 0.045 mm; (**f**) −0.045 +0 mm.

Analysis of the data presented in Figure 1 by size classes allows us to evaluate the forms of aggregates in the studied material, as well as show the presence of microspheres in fine classes. The main component of ash and slag composition is slag of black, gray, and less often whitish-gray colors; porous, pumice, spongy, and dense textures; as well as slag in the form of fragments.

The particles in the ash composition are heterogeneous both in shape and surface condition; the heterogeneity is preserved in different groups of size fractions. All particles can be divided into two types:

- Spheroids of various diameters formed as a result of the solidification of molten particles suspended in the flue gas stream (several types depending on the composition are fixed). It is established that in the fine class, there is a significant amount of particles smaller than 5 microns;
- unmelted and partially melted.

In the composition of ash and slag, up to 20% is magnetic particles, and aluminosilicate particles are also present. Additionally, such elements as arsenic, sulfur, potassium, manganese, titanium, copper, nickel, etc., are also present.

*2.2. Magnetic Separation*

Magnetic fractionation was carried out on a Davis Tube Tester 298 SE (NPK "Mekhanobr-Tekhnika" (JSC), St. Petersburg, Russia) to evaluate the distribution of Fe into fractions depending on the magnetic induction and to determine the possibility of using high-gradient magnetic separation. The initial sample of size −0.5 + 0 mm weighing 50 g in pulp form was separated at different current intensities (1, 2, 3, 4, 5, and 6 A, which correspond to 0.14, 0.25, 0.345, 0.422, 0.483, and 0.54 Tesla). In the first experiment (I = 1 A), magnetic and non-magnetic fractions are separated. The feed of subsequent experiments (with increasing current intensity) is the nonmagnetic fraction of the previous experiment. As a result, 7 products were obtained (6 magnetic fractions and 1 non-magnetic fraction), which were dried and analyzed.

Experiments on high-gradient magnetic separation were carried out on a vertical pulsation high-gradient magnetic separator SLon 100 (Outotec, Espoo, Finland) (Figure 2). Samples of size -0.8 + 0 mm weighing 100 g were prepared.


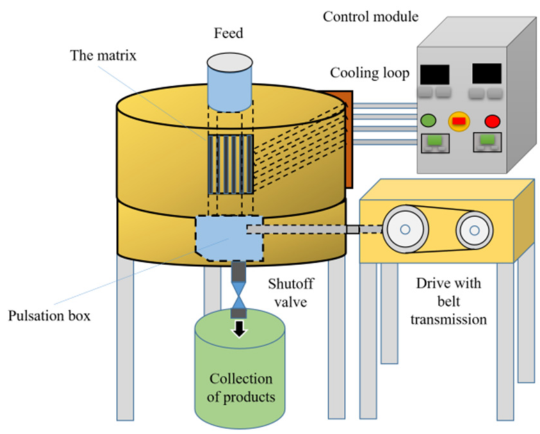


**Figure 2.** Vertical pulsation high-gradient magnetic separator SLon 100: (**a**) general view, (**b**) separator scheme.

The separation of the magnetic fraction is carried out by passing the pulp through a rod matrix (magnetic particles are retained) under a strong magnetic field (Figure 3). The magnetic system of the SLon 100 separator uses a rod matrix made of rods with a diameter of 1–6 mm for different feed material sizes. The rods are arranged perpendicular to the magnetic field at an equal distance in order to ensure optimal field intensity and reduce the possibility of particle entrapment.

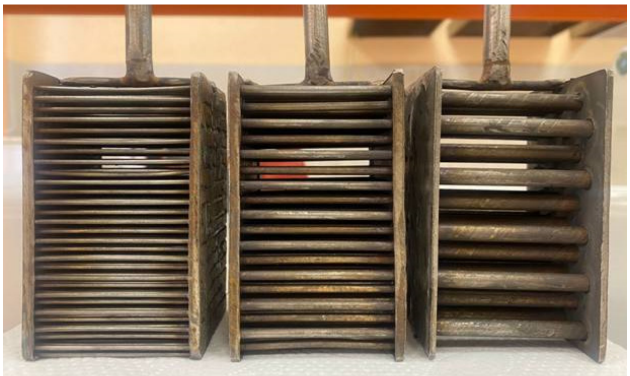

**Figure 3.** Matrices with rods arranged in staggered order.

The magnetic force $(F_m)$ acting on the particle from the rod side (one of the main factors of magnetic separation) in the cylindrical coordinate system can be calculated by the following formula [41–43]:

$$F_m = \sqrt{F_r^2 + F_\tau^2} \quad (1)$$

where $F_r$ and $F_\tau$ are the radial and tangential components of the magnetic force $F_m$.

$$F_r = -\frac{1}{2}\mu_0 K_p V_p M H \frac{a^2}{r^3}\left(cos2\alpha + \frac{M}{H}\frac{a^2}{r^2}\right) \quad (2)$$

$$F_\tau = -\frac{1}{2}\mu_0 K_p V_p M H \frac{a^2}{r^3} sin2\alpha \quad (3)$$

where $M$ is the induced magnetization of the particle; $r$ is the distance from the axis of the rod to the center of the particle; $\mu_0$ is the permittivity of the media; $a$ is the radius of the rod; $H$ is the value of magnetic field intensity; $K_p$ is the magnetic susceptibility of the particle; $V_p$ is the volume of the particle; $\alpha$ is the angle between the direction of the radial component of the magnetic force and the x-axis; and $H$ is the magnetic field intensity.

For the simplest condition, the sample grain size is homogeneous, and the particles differ only in composition; it is possible to denote the parameters characterizing the particle by

$$W_p = K_p M V_p, \text{ then } W_p = f(H) \quad (4)$$

To understand the character of the dependence ($W^p = f(H)$), studies have been carried out based on the accumulated database of investigations of the action of magnetic forces on a mineral particle in the working zone of a high-gradient magnetic separator (rods) and using the given Equations (1)–(4) (Figure 4).

Investigations on magnetic separation were carried out in one stage by varying the following parameters: magnetic induction (0.2, 0.5, 1.1 Tesla), diameter of matrix rods (1, 3, 6 mm), and pulp pulsation (200, 250, 300 min$^{-1}$). Also, to increase the separation efficiency, Polypam and Flotfloc flocculants from Flotent Chemicals were used with varying consumptions of 1, 10, and 100 g/t.

All experimental investigations were carried out at least three times to increase reliability. The tables summarize the average results of the measurements of the elemental composition of the samples.

All the obtained products were dried at 105 °C, weighed, and analyzed using a Shimadzu EDX 700 X-ray fluorescence analyzer and a Vega 3 LMH scanning electron microscope. To analyze the samples using X-ray fluorescence analysis, representative samples for analysis were taken from the initial samples and from all beneficiation products with a mass of 5 g. The samples were put into special cuvettes and covered with mylar film. At least three samples were taken for each product. The obtained samples were analyzed at least three times. For the investigation of samples using scanning electron microscopy, representative samples of 2 g were taken from the initial ash and beneficiation products. The obtained samples were put on carbon tape and carburized to avoid sample lightening. The obtained samples were placed in a microscope and analyzed by local XRF.

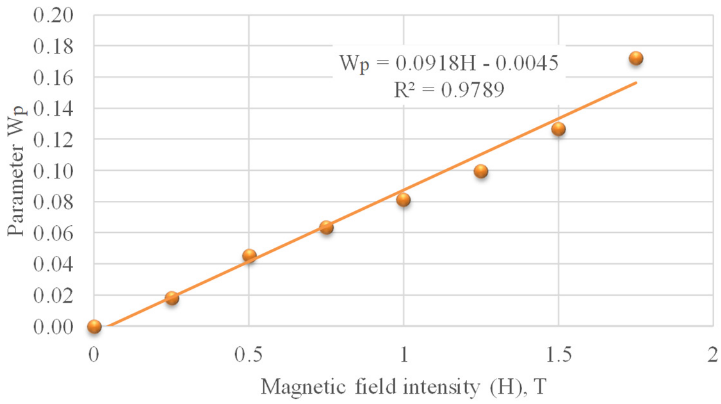


**Figure 4.** Dependence of the parameter characterizing the particle property on the magnetic field intensity ($W_p = f(H)$).

## 3. Results

Magnetic fractionation was carried out on a Davis Tube Tester at different current intensities. These investigations are necessary to assess the possibility and feasibility of the recovery of valuable iron-containing components from ash and slag by magnetic methods. The results are presented in Table 2 and Figure 5.

**Table 2.** Results of X-ray fluorescence analysis of magnetic fractionation products.

| Product | Yield, % | Fe | Si | S | As | Al | Ca | Sb | K | Mn | Zn | Cu | Ni | Sr |
|---|---|---|---|---|---|---|---|---|---|---|---|---|---|---|
| | | Content, % | | | | | | | | | | | | |
| Magnetic fraction (1 A) | 1.04 | 29.55 | 16.23 | 2.53 | 2.75 | 1.17 | 2.18 | 1.03 | 0.81 | 0.14 | 0.076 | 0.069 | 0.034 | 0.011 |
| Magnetic fraction (2 A) | 4.32 | 32.82 | 15.84 | 3.29 | 3.05 | 1.44 | 3.19 | 1.41 | 1.02 | 0.21 | 0.073 | 0.121 | 0.039 | 0.014 |
| Magnetic fraction (3 A) | 2.02 | 33.65 | 16.43 | 2.58 | 3.38 | 1.61 | 3.48 | 2.22 | 0.77 | 0.25 | 0.071 | 0.068 | 0.038 | 0.013 |
| Magnetic fraction (4 A) | 3.68 | 30.52 | 15.85 | 2.89 | 2.77 | 2.32 | 3.94 | 1.88 | 1.05 | 0.19 | 0.073 | 0.069 | 0.033 | 0.014 |
| Magnetic fraction (5 A) | 4.96 | 23.79 | 16.87 | 4.17 | 3.07 | 2.28 | 1.84 | 0.82 | 1.75 | 0.13 | 0.049 | 0.047 | 0.021 | 0.01 |
| Magnetic fraction (6 A) | 12.6 | 28.41 | 14.59 | 3.13 | 3.21 | 1.94 | 2.06 | 1.61 | 0.84 | 0.17 | 0.084 | 0.08 | 0.032 | 0 |
| Non-magnetic fraction | 71.38 | 29.97 | 15.98 | 2.38 | 3.55 | 2.45 | 3.62 | 2.16 | 0.8 | 0.19 | 0.073 | 0.071 | 0.037 | 0.014 |
| Total: | 100 | 29.68 | 15.85 | 2.63 | 3.42 | 2.30 | 3.31 | 1.97 | 0.87 | 0.19 | 0.07 | 0.073 | 0.036 | 0.012 |
| **Product** | **Yield, %** | **Recovery, %** | | | | | | | | | | | | |
| Magnetic fraction (1 A) | 1.04 | 1.035 | 1.065 | 1.002 | 0.836 | 0.529 | 0.685 | 0.543 | 0.968 | 0.783 | 1.080 | 0.984 | 0.996 | 0.954 |
| Magnetic fraction (2 A) | 4.32 | 4.777 | 4.317 | 5.410 | 3.851 | 2.706 | 4.163 | 3.090 | 5.063 | 4.876 | 4.309 | 7.166 | 4.745 | 5.046 |
| Magnetic fraction (3 A) | 2.02 | 2.290 | 2.094 | 1.984 | 1.996 | 1.415 | 2.123 | 2.275 | 1.787 | 2.714 | 1.960 | 1.883 | 2.162 | 2.191 |
| Magnetic fraction (4 A) | 3.68 | 3.784 | 3.680 | 4.048 | 2.979 | 3.714 | 4.380 | 3.510 | 4.440 | 3.758 | 3.671 | 3.481 | 3.420 | 4.298 |
| Magnetic fraction (5 A) | 4.96 | 3.976 | 5.279 | 7.873 | 4.451 | 4.920 | 2.757 | 2.064 | 9.973 | 3.466 | 3.321 | 3.196 | 2.934 | 4.138 |
| Magnetic fraction (6 A) | 12.6 | 12.061 | 11.598 | 15.013 | 11.822 | 10.634 | 7.840 | 10.292 | 12.160 | 11.512 | 14.462 | 13.818 | 11.356 | 0.000 |
| Non-magnetic fraction | 71.38 | 72.077 | 71.966 | 64.669 | 74.065 | 76.081 | 78.052 | 78.225 | 65.609 | 72.892 | 71.198 | 69.473 | 74.386 | 83.373 |
| Total: | 100 | 100 | 100 | 100 | 100 | 100 | 100 | 100 | 100 | 100 | 100 | 100 | 100 | 100 |

The magnetic fraction is represented by small crystals of iron-bearing minerals and their fragments, often melted from the edges or pelletized, as well as small fragments of flattened veins. Interpretation of the results presented in Figure 5 shows that the microspheres observed in the concentrates consist mainly of Fe. Si, S, Ca (5a), and Si, S (5b) are noted as impurities. The detected microspheres have a sufficiently large size of 20–80 microns. It is worth noting that at a current strength of 2 A, the recovery of larger particles containing more iron occurs than at a current strength of 3 A.

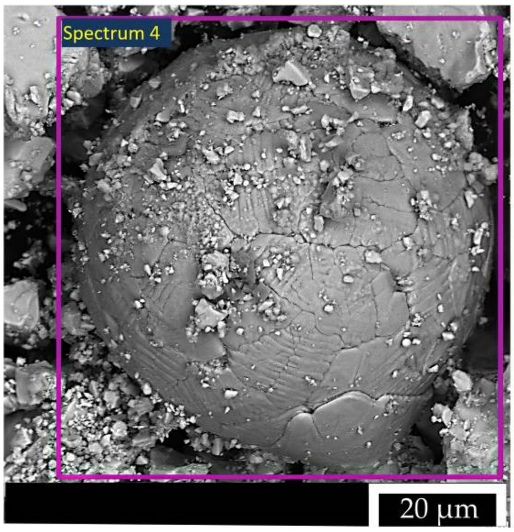


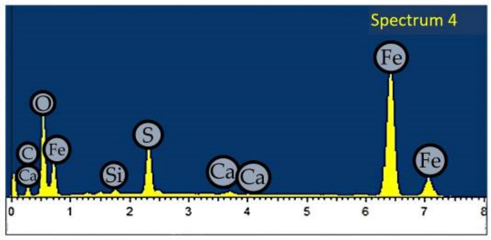


| Spectrum No. | Content, wt. % | | | | |
|---|---|---|---|---|---|
| | O | Si | S | Ca | Fe |
| Spectrum 4 | 23.03 | 0.59 | 6.24 | 0.46 | 69.68 |

(**a**)

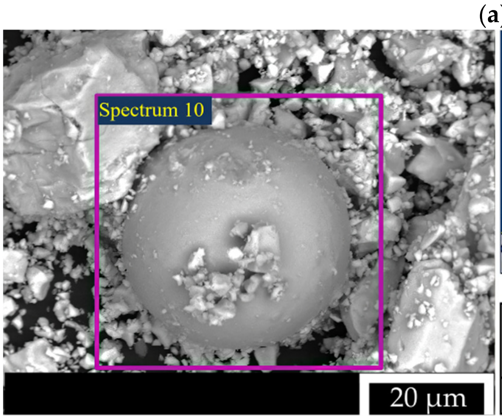


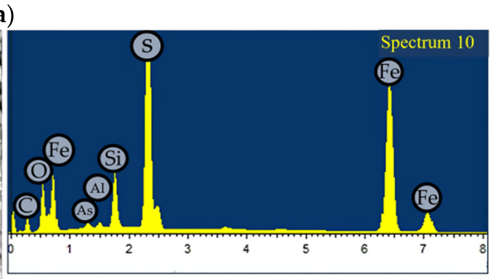


| Spectrum No. | Content, wt. % | | | |
|---|---|---|---|---|
| | O | Si | S | Fe |
| Spectrum 10 | 12.34 | 0.93 | 25.6 | 61.13 |

(**b**)

**Figure 5.** Electron image of magnetic microspheres in the separation products: (**a**) iron-containing sphere associated with intermetallics in the magnetic fraction obtained at a current strength of 2 A, (**b**) iron-containing sphere associated with intermetallics in the magnetic fraction obtained at a current of 3 A.

The obtained results showed that the distribution of iron is quite equal in all fractions, but microspheres, which include high-magnetic iron minerals associated with intermetallics, are mainly concentrated in the magnetic fractions obtained at current values of 2, 3, and 4 A (0.25, 0.345, and 0.422 Tesla, respectively). It can be supposed that iron in the compounds has different valence forms and different magnetic properties [44]. At the same time, particles containing low-magnetic iron and aluminum were not found in the separated magnetic fractions. The iron content in the non-magnetic fraction is explained by the presence of complex particles including Ca, Fe, K, Al, Si, S, and rare metals. These particles have a reduced magnetic susceptibility. High-gradient magnetic separation has been proposed to separate such particles (microspheres) from fine materials.

Investigations on the influence of different parameters and settings of the magnetic separator (including matrix size, field strength, and pulsation frequency) on the characteristics of recovery and concentration of the target component were carried out on a high-gradient magnetic separator with variation of technological parameters and modes.

The I optimal experiment plan with additional central points was made (Table 3). Plans of this type are best suited for determining the optimal parameters and initializing the response surface. As a response was used, the recovery parameter was calculated as the arithmetic mean of three measurements of the obtained concentrate (the obtained values lie within three sigma).

**Table 3.** Experimental design.

| | | Factor 1 | Factor 2 | Factor 3 | Response 1 |
|---|---|---|---|---|---|
| **Group** | **Run** | **a: Field Density** | **b: Pulsation Mode** | **C: Matrix** | **Recovery** |
| | | **T** | **1/min** | | **%** |
| 1 | 1 | 0.2 | 200 | Matrix 6 mm | 71.82 |
| 1 | 2 | 0.2 | 200 | Matrix 3 mm | 66.81 |
| 1 | 3 | 0.2 | 200 | Matrix 1.5 mm | 61.38 |
| 2 | 4 | 1.1 | 200 | Matrix 3 mm | 76.81 |
| 2 | 5 | 1.1 | 200 | Matrix 1.5 mm | 74.52 |
| 3 | 6 | 1.2 | 250 | Matrix 6 mm | 77.04 |
| 3 | 7 | 1.2 | 250 | Matrix 1.5 mm | 75.62 |
| 4 | 8 | 0.2 | 300 | Matrix 3 mm | 72.47 |
| 4 | 9 | 0.2 | 300 | Matrix 6 mm | 74.69 |
| 4 | 10 | 0.2 | 300 | Matrix 1.5 mm | 65.03 |
| 5 | 11 | 1.1 | 300 | Matrix 6 mm | 81.92 |
| 5 | 12 | 1.1 | 300 | Matrix 3 mm | 78.79 |
| 5 | 13 | 1.1 | 300 | Matrix 1.5 mm | 76.99 |
| 6 | 14 | 0.5 | 250 | Matrix 1.5 mm | 70.23 |
| 6 | 15 | 0.5 | 250 | Matrix 3 mm | 73.51 |
| 7 | 16 | 0.5 | 200 | Matrix 6 mm | 75.11 |
| 7 | 17 | 0.5 | 200 | Matrix 1.5 mm | 64.68 |
| 8 | 18 | 0.5 | 250 | Matrix 3 mm | 73.29 |
| 8 | 19 | 0.5 | 250 | Matrix 6 mm | 75.23 |

The Restricted Maximum Likelihood (REML) analysis and calculated Kenward–Roger *p*-values are summarized in Table 4.

**Table 4.** Analyzing the significance of the model coefficients.

| Source | Term df | Error df | F-Value | *p*-Value | |
|---|---|---|---|---|---|
| Whole-plot | 3 | 2.95 | 24.14 | 0.0140 | significant |
| a-Field density | 1 | 3.24 | 53.50 | 0.0040 | |
| b-Pulsation mode | 1 | 3.28 | 10.25 | 0.0436 | |
| ab | 1 | 3.15 | 0.0015 | 0.9713 | |
| Subplot | 8 | 3.65 | 11.51 | 0.0208 | significant |
| C-Matrix | 2 | 4.29 | 26.06 | 0.0040 | |
| aC | 2 | 4.10 | 8.00 | 0.0385 | |
| bC | 2 | 4.02 | 0.0934 | 0.9127 | |
| abC | 2 | 3.86 | 1.23 | 0.3855 | |

*p*-values less than 0.0500 indicate that the model conditions are significant. In this case, a, b, C, and aC are significant model terms. Values greater than 0.1000 indicate that the model terms are not significant.

As a result, adequate process models are obtained:

- matrix rod diameter = 6 mm

$$Recovery = 71.906 - 11.396a + 0.0047b + 0.062a{\cdot}b, \quad (5)$$

где a—field density, b—pulsation mode;

- matrix rod diameter = 3 mm

$$Recovery = 52.127 + 19.041a + 0.065b - 0.0401a{\cdot}b, \quad (6)$$

- matrix rod diameter = 1.5 mm

$$Recovery = 49.460 + 17.179a + 0.047b - 0.017a{\cdot}b. \quad (7)$$

Figure 6 shows the results of high-gradient magnetic separation with variations of technological parameters.

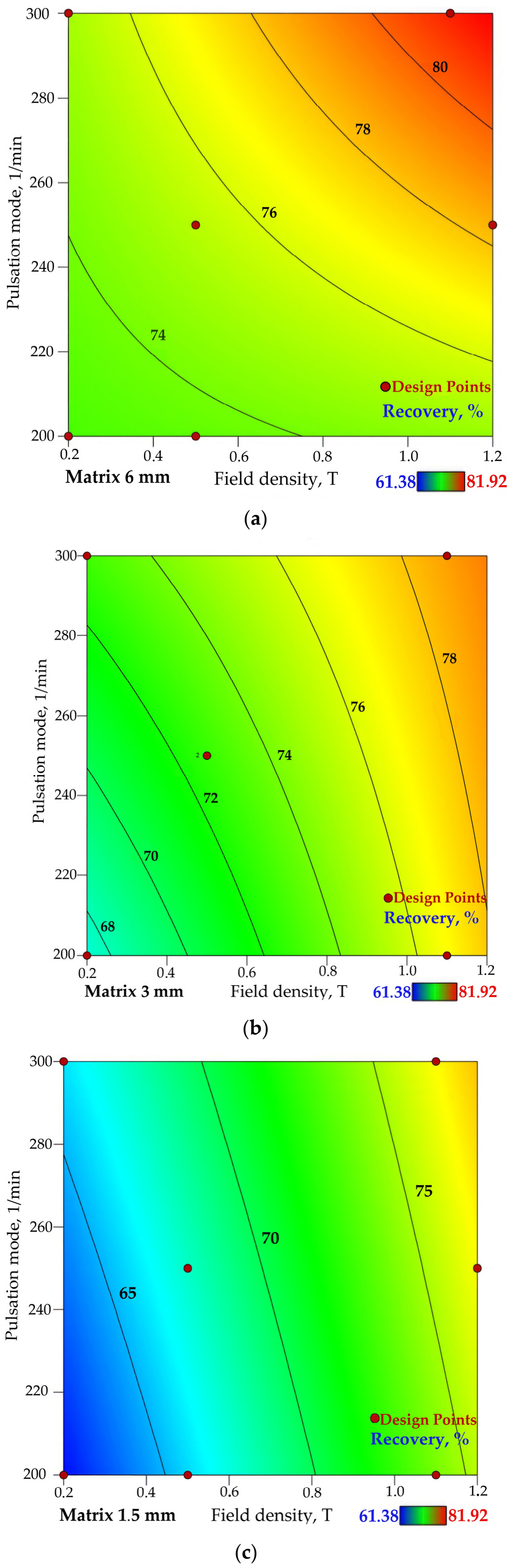


**Figure 6.** Graphical interpretation of the obtained results of high-gradient magnetic separation: (**a**) diameter of matrix rods = 6 mm; (**b**) diameter of matrix rods = 3 mm; (**c**) diameter of matrix rods = 1.5 mm.

The influence of technological parameters on iron recovery is presented in Figure 7.

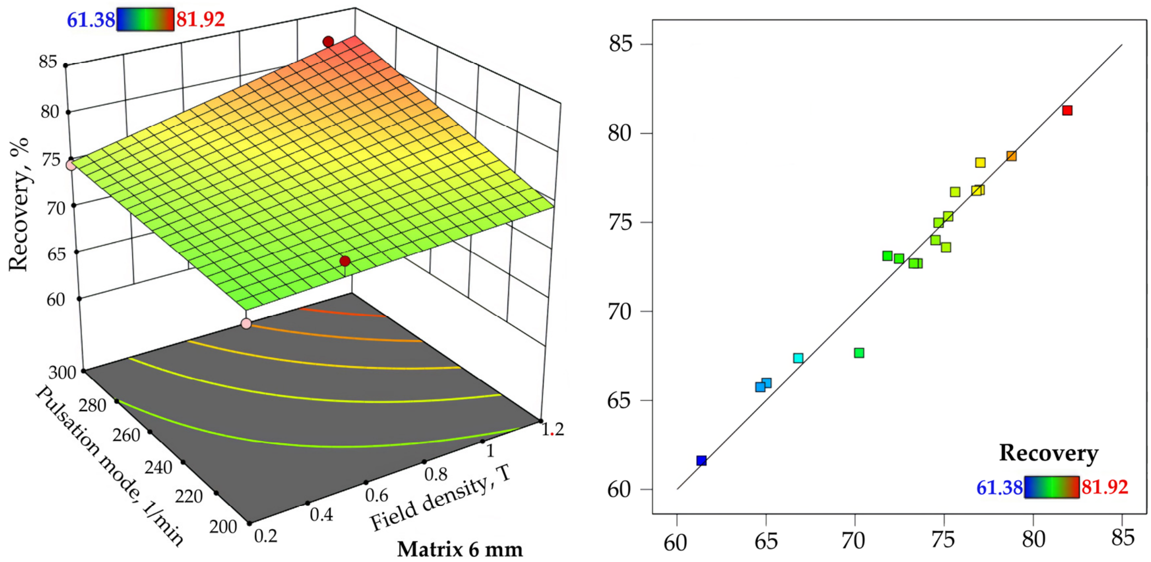


| | | | | |
|---|---|---|---|---|
| **Std. Dev.** | 1.58 | | **$R^2$** | 0.9692 |
| **Mean** | 72.94 | | **Adjusted $R^2$** | 0.8891 |
| **C.V. %** | 2.16 | | | |

**Figure 7.** Three-dimensional response surface and statistical characteristics of the model.

The search for the largest response value was conducted using the Levenberg–Marquardt method (Figure 8).

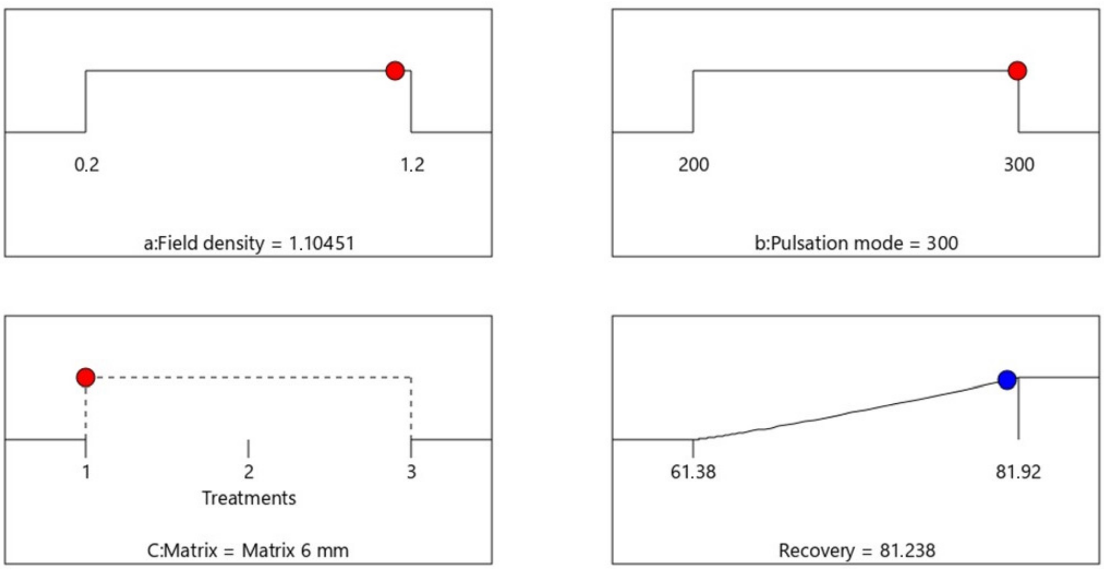


| Solution | Predicted Mean | Predicted Median | Total Std Dev | SE Mean | Error df | 95% CI low for Mean | 95% CI high for Mean | 95% TI low for 99% Pop | 95% TI high for 99% Pop |
|---|---|---|---|---|---|---|---|---|---|
| Recovery | 81.238 | 81.238 | 1.16814 | 1.04248 | 4.64673 | 78.4958 | 83.9802 | 72.5653 | 89.9107 |

**Figure 8.** Results of optimization of iron recovery process in high-gradient magnetic separation.

The highest magnetic force can be obtained by using a 1.5 mm matrix, while the highest gradient can be obtained by using a 6 mm matrix. In [45], it is shown that the use of a larger matrix results in a purer concentrate in terms of the iron content of the concentrate, which is particularly evident for particles smaller than 37 µm. This agrees well with the obtained results, as the recovered microspheres are 2–15 µm in size.

According to the results of our investigation, iron recovery in the concentrate increases with the increase in size due to the increase in content. The above beneficiation parameters confirm that the unique design of the Slon separator, as well as the higher magnetic field strength, allows us to significantly increase the recovery of iron in the concentrate. Thus, because of this research, it was established that the best results are achieved with the following parameters of operation of the high-gradient magnetic separator: magnetic induction 1.1 Tesla, diameter of matrix rods 6 mm, pulsation frequency 300 $min^{-1}$.

In order to increase the recovery of iron in the concentrate, another series of experiments with the use of flocculants was performed. The analysis of previously published works showed that during the magnetic separation of fine-grained ash and slag materials, the addition of flocculants allows an increase in the recovery of valuable components in the magnetic fraction [46]. When using flocculants and magnetic particles together, the mechanism of heteroflocculation is intensified. This occurs because of the binding of fine sludge by flocculant molecules, as well as the formation of "soft" flocculates around magnetic centers due to the selective action of the reagent, which increases the rate of coagulation [47]. Due to the increase in tension on additional particles of magnetite, there is an increase in the degree of the magnetic susceptibility of magnetic particles in the initial material. The flocculants Polypam and Flotfloc were chosen for this research because they are universal and can be used in rather complex slurries (acidic, neutral, and alkaline media). The consumption rate was varied to 1, 10, and 100 g/t. The results are presented in Figure 9.

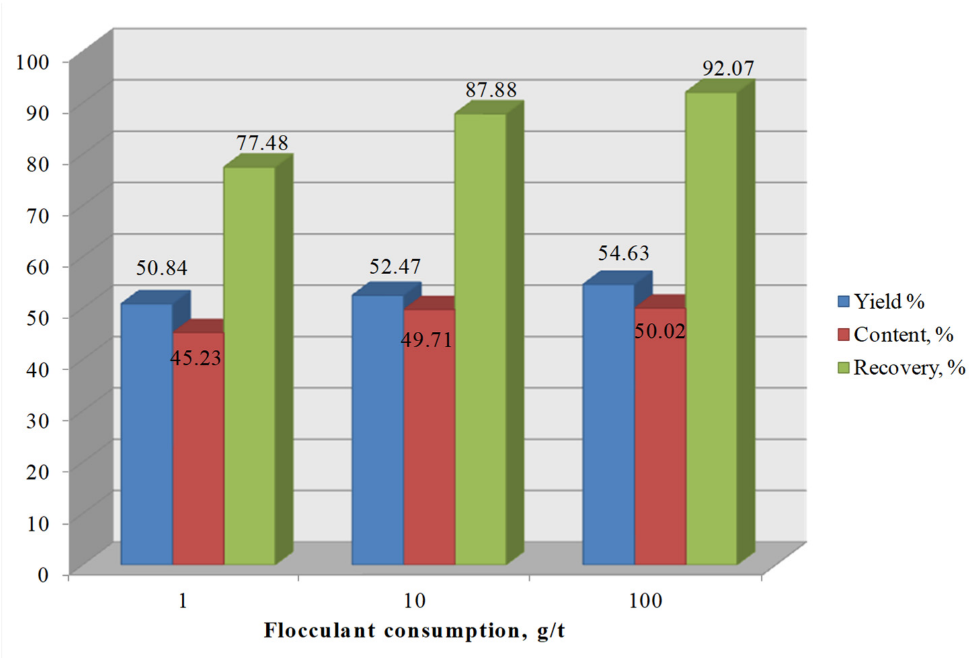


(**a**)

**Figure 9.** *Cont.*

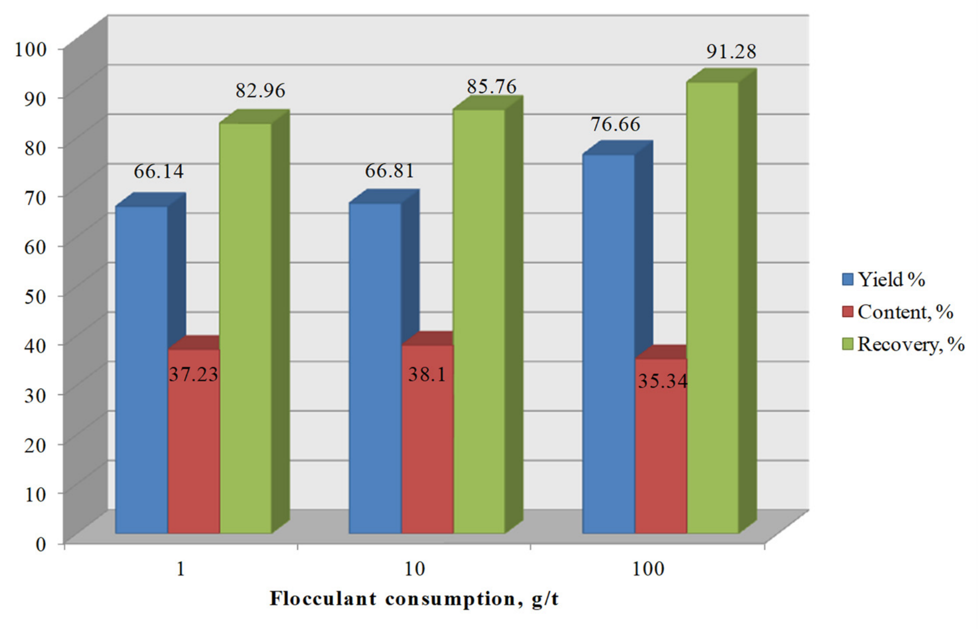


(**b**)

**Figure 9.** Investigation of the influence of flocculant addition: (**a**) Flotifloc; (**b**) Polypam.

The obtained results showed that the addition of the Flotifloc flocculant in an amount of 100 g/t allows us to obtain an iron content in the concentrate of 50% with a recovery of 92%. The addition of the Polypam flocculant increases the yield of the magnetic fraction, but the content decreases.

The conducted investigations made it possible to establish the optimal mode of magnetic concentrate production (Figure 10 and Table 5) on the high-gradient magnetic separator SLon.

**Table 5.** Results of elemental composition of ash after magnetic beneficiation (Figure 10).

| | Content, wt. % | | | | |
|---|---|---|---|---|---|
| | **O** | **Al** | **Si** | **Ca** | **Fe** |
| Spectrum 1 | 32.34 | 9.2 | 21.31 | 3.13 | 34.02 |
| Spectrum 2 | 30.83 | 6.62 | 16.91 | 2.2 | 43.44 |
| Spectrum 3 | 33.05 | 9.84 | 16.17 | 0.85 | 40.09 |
| Spectrum 4 | 30.12 | | | | 69.88 |

Analysis of the data shown in Figure 10 shows that low-magnetic and aluminosilicate iron-containing microspheres were detected in the concentrates obtained on the established regime for high-gradient separation with the application of scanning electron microscopy. The composition of the microspheres is summarized in Table 3. Interpretation of the results shows that the detected microspheres are mainly composed of Al, Si, Ca, and Fe. At the same time, microspheres representing iron oxides were detected (Figure 10, spectrum 4). Thus, the presence of low-magnetic and aluminosilicate iron-containing microspheres is confirmed, which agrees well with the results of earlier studies [22,48]. It is also worth noting that the sizes of extracted particles of valuable components with low values of magnetic susceptibility (less than 15 microns) are in good agreement with the work [49], in which the application of a high-gradient separator for sludge beneficiation is justified. The possibility of their extraction into the magnetic product using high-gradient magnetic separation is also proven.

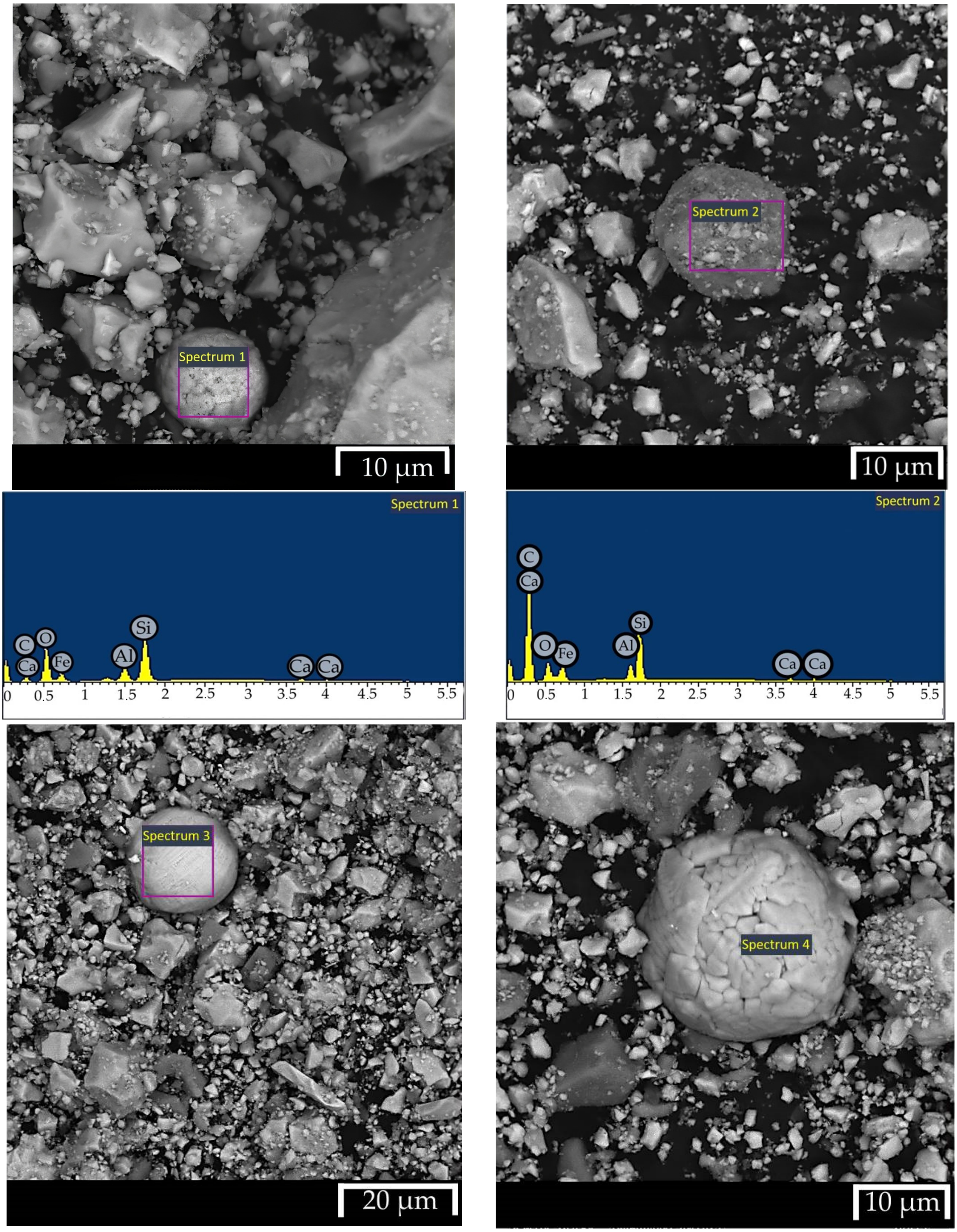


**Figure 10.** *Cont*.

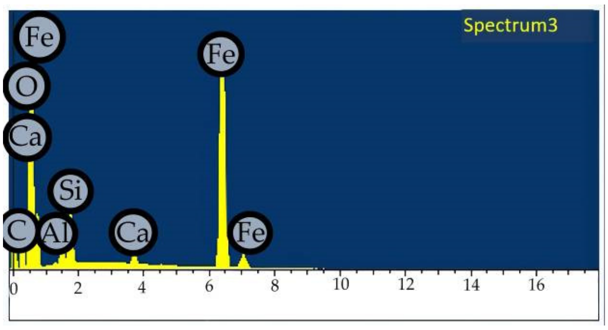


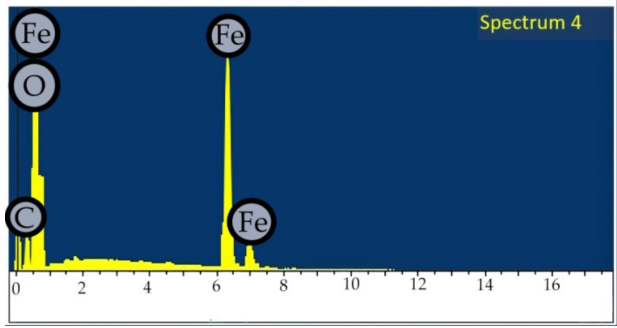


**Figure 10.** Results of research of ash and slag after magnetic beneficiation under optimal separation conditions using scanning electron microscopy.

The concentrate contains magnetic (low-magnetic iron) and aluminosilicate microspheres with sizes from 2 to 15 microns. It is practically impossible to recover such materials by standard beneficiation methods [35]. As a result of this research, it was established that for the beneficiation of ash and slag material by the method of high-gradient magnetic separation, the optimal parameters are magnetic induction 1.1 Tesla, diameter of matrix rods 6 mm, pulsation frequency 300 min$^{-1}$, and consumption of flocculant Flotifloc 100 g/t.

Thus, to recover microspheres of different compositions and sizes, a sequential scheme of magnetic concentration is recommended: magnetic separation in a weak magnetic field (concentrate contains high-magnetic iron-containing microspheres associated with intermetallics) and high-gradient separation of tailings (concentrate contains low-magnetic iron-containing and aluminosilicate microspheres ranging in size from 2 to 15 microns) (Figure 11).

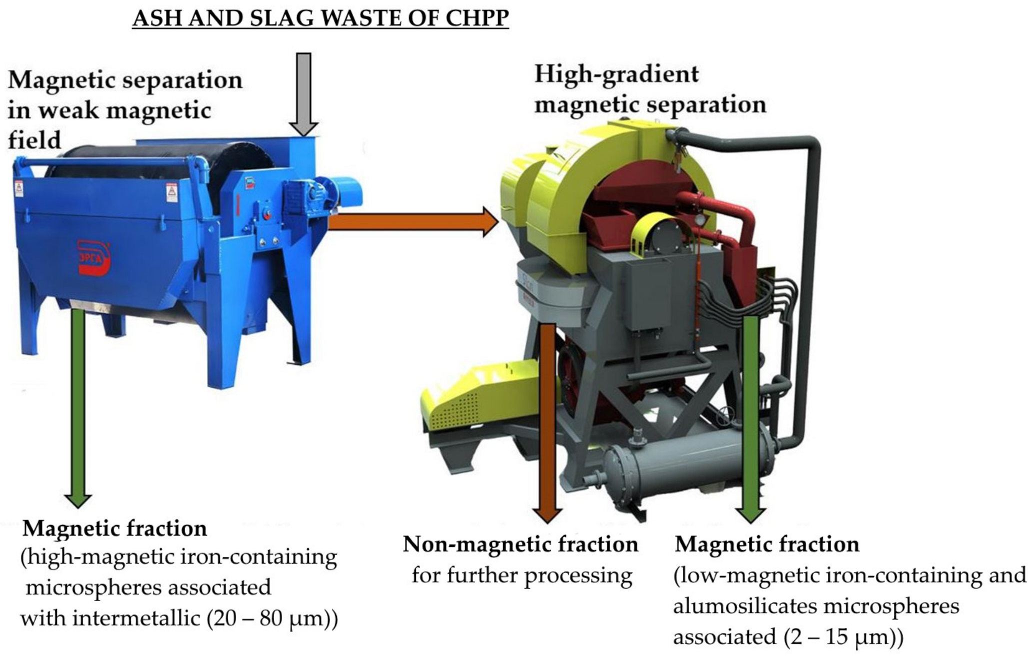


**Figure 11.** Topology of the scheme of magnetic beneficiation of ash and slag waste from CHPP.

The materials obtained by this technology have unique properties and can serve as raw materials to produce sorbents, magnetic carriers, etc.

## 4. Conclusions

This paper presents the research results aimed at substantiating the possibility of using magnetic beneficiation methods (including high-gradient magnetic separation) in the processing of ash and slag wastes from CHPPs, as well as the optimization of the parameters of the magnetic beneficiation process. Ash and slag wastes were chosen as objects of research on the principle of the presence of valuable components such as iron, aluminum, etc.

Based on magnetic fractioning studies on a Davis tube tester, it was found that iron is present in all fractions in approximately the same amount, but only three fractions obtained at current values of 2, 3, and 4 A (0.25, 0.345, and 0.422 Tesla, respectively), concentrated magnetic microspheres, contained high-magnetic iron minerals associated with intermetallics ranging in size from 20 to 80 microns.

This is due to the fact that iron is included in the compounds in different valence forms and has different magnetic properties. The results of the conducted research proved the principal possibility of using the pulsation high-gradient magnetic separator Slon. Its unique design (high magnetic field intensity, pulsation of the pulp) allows us to separate finely accumulated particles quite effectively. New features of magnetic and aluminosilicate microsphere recovery were established during the complex study of the parameters of operation of a high-gradient magnetic separator (joint influence of the size of matrix rods and magnetic induction).

The proposed regime (magnetic induction 1.1 Tesla, diameter of matrix rods 6 mm, pulsation frequency 300 $min^{-1}$, Flotifloc 100 g/t flocculant consumption) allows for one stage to obtain an iron ore product with an iron content of 50% and a recovery of 92%. With the use of scanning electron microscopy, it was established that at these parameters, the main portion of microspheres, which contain low-magnetic iron minerals and aluminosilicates with sizes ranging from 2 to 15 microns, is recovered in the magnetic fraction.

As a result of the performed research, the topology of the technological scheme of magnetic beneficiation for obtaining products with high added value (high- and low-magnetic iron-containing and aluminosilicate microspheres) was proposed. The proposed solution will not only allow us to obtain materials unique in their technological properties but also to reduce the environmental load in areas of ash dumps.

**Author Contributions:** T.A. conceived and designed the experiments and analyzed the data; N.N. and A.R. implemented and processed the analysis results; A.A., V.A. and E.P. performed the experiments; D.C. analyzed the data. All authors have read and agreed to the published version of the manuscript.

**Funding:** This work was carried out with a grant from the Russian Science Foundation (Project N 23-47-00109).

**Data Availability Statement:** Data are contained within the article.

**Conflicts of Interest:** The authors declare no conflicts of interest.

## References

1. Meng, J.; Liao, W.; Zhang, G. Emerging $CO_2$-Mineralization Technologies for Co-Utilization of Industrial Solid Waste and Carbon Resources in China. *Minerals* **2021**, *11*, 274. [CrossRef]
2. Grigoryev, L.M.; Kheifets, E.A. Oil market: Conflict between recovery and energy transition. *Vopr. Ekon.* **2022**, *9*, 5–33. [CrossRef]
3. Aleksandrova, T.; Nikolaeva, N.; Kuznetsov, V. Thermodynamic and Experimental Substantiation of the Possibility of Formation and Extraction of Organometallic Compounds as Indicators of Deep Naphthogenesis. *Energies* **2023**, *16*, 3862. [CrossRef]
4. Nepsha, F.S.; Varnavskiy, K.A.; Voronin, V.A.; Zaslavskiy, L.S.; Liven, A.S. Integration of renewable energy at coal mining enterprises: Problems and prospects. *J. Min. Inst.* **2023**, *261*, 455–469.
5. Dvoynikov, M.V.; Leusheva, E.L. Modern trends in hydrocarbon resources development. *J. Min. Inst.* **2022**, *258*, 879–880.
6. Bazhin, V.Y.; Kuskov, V.B.; Kuskova, Y.V. Processing of low-demand coal and other carbon-containing materials for energy production purposes. *Inz. Miner.* **2019**, *21*, 195–198. [CrossRef]
7. Shklyarskiy, Y.E.; Skamyin, A.N.; Jiménez Carrizosa, M. Energy efficiency in the mineral resources and raw materials complex. *J. Min. Inst.* **2023**, *261*, 323–324.
8. Litvinenko, V.S.; Petrov, E.I.; Vasilevskaya, D.V.; Yakovenko, A.V.; Naumov, I.A.; Ratnikov, M.A. Assessment of the role of the state in the management of mineral resources. *J. Min. Inst.* **2022**, *259*, 95–111. [CrossRef]
9. Litvinenko, V.S. Digital Economy as a Factor in the Technological Development of the Mineral Sector. *Nat. Resour. Res.* **2020**, *29*, 1521–1541. [CrossRef]

10. Albalate, D.; Bel, G.; Teixidó, J.J. The Influence of Population Aging on Global Climate Policy. *Popul. Environ.* **2023**, *45*, 13. [CrossRef]
11. Our World in Data. Available online: https://ourworldindata.org/electricity-mix (accessed on 19 November 2023).
12. Plakitkin, Y.A.; Plakitkina, L.S.; Dyachenko, K.I. Coal as the basis of a great civilization leap and new opportunities for world development. *Ugol'* **2022**, *8*, 77–83. [CrossRef]
13. Chukaeva, M.A.; Matveeva, V.A.; Sverchkov, I.P. Complex processing of high-carbon ash and slag waste. *J. Min. Inst.* **2022**, *253*, 97–104. [CrossRef]
14. Yatsenko, E.A.; Goltsman, B.M.; Trofimov, S.V.; Lazorenko, G.I. Processing of Ash and Slag Waste from Coal Fuel Combustion at CHPPs in the Arctic Zone of Russia with Obtaining Porous Geopolymer Materials. *Therm. Eng.* **2022**, *69*, 615–623. [CrossRef]
15. Yatsenko, E.A.; Smolii, V.A.; Klimova, L.V.; Gol'tsman, B.M.; Ryabova, A.V.; Golovko, D.A.; Chumakov, A.A. Solid Fuel Combustion Wastes at CHPP in the Arctic Zone of the Russian Federation: Utility in Eco-Geopolymer Technology. *Glass Ceram.* **2022**, *78*, 374–377. [CrossRef]
16. Marinina, O.; Nevskaya, M.; Jonek-Kowalska, I.; Wolniak, R.; Marinin, M. Recycling of Coal Fly Ash as an Example of an Efficient Circular Economy: A Stakeholder Approach. *Energies* **2021**, *14*, 3597. [CrossRef]
17. Pukhov, S.A.; Kiseleva, S.P. Involvement in the economic turnover of ash and slag waste of thermal powerplants in the interests of eco-oriented economic development. *Russ. J. Resour. Conserv. Recycl.* **2020**, *7*, 10. (In Russian) [CrossRef]
18. Dyk, J.C.V.; Benson, S.A.; Laumb, M.L.; Waanders, B. Coal and Coal Ash Characteristics to Understand Mineral Transformations and Slag Formation. *Fuel* **2009**, *88*, 1057–1063. [CrossRef]
19. Uliasz-Bochenczyk, A.; Mokrzycki, E. Fly Ashes from Polish Power Plants and Combined Heat and Power Plants and Conditions of Their Application for Carbon Dioxide Utilization. *Chem. Eng. Res. Des.* **2006**, *84*, 837–842. [CrossRef]
20. Basu, M.; Pande, M.; Bhadoria, P.B.S.; Mahapatra, S.C. Potential Fly-Ash Utilization in Agriculture: A Global Review. *Prog. Nat. Sci.* **2009**, *19*, 1173–1186. [CrossRef]
21. Bhatt, A.; Priyadarshini, S.; Mohanakrishnan, A.A.; Abri, A.; Sattler, M.; Techapaphawit, S. Physical, Chemical, and Geotechnical Properties of Coal Fly Ash: A Global Review. *Case Stud. Constr. Mater.* **2019**, *11*, e00263. [CrossRef]
22. Vereshchak, M.; Manakova, I.; Shokanov, A.; Sakhiyev, S. Mössbauer Studies of Narrow Fractions of Fly Ash Formed after Combustion of Ekibastuz Coal. *Materials* **2021**, *14*, 7473. [CrossRef] [PubMed]
23. Ma, Z.; Shan, X.; Cheng, F. Distribution Characteristics of Valuable Elements, Al, Li, and Ga, and Rare Earth Elements in Feed Coal, Fly Ash, and Bottom Ash from a 300 MW Circulating Fluidized Bed Boiler. *ACS Omega* **2019**, *4*, 6854–6863. [CrossRef] [PubMed]
24. Hu, X.; Huang, X.; Zhao, H.; Liu, F.; Wang, L.; Zhao, X.; Gao, P.; Li, X.; Ji, P. Possibility of Using Modified Fly Ash and Organic Fertilizers for Remediation of Heavy-Metal-Contaminated Soils. *J. Clean. Prod.* **2021**, *284*, 124713. [CrossRef]
25. Loya, M.I.M.; Rawani, A.M. A review: Promising applications for utilization of fly ash. *Int. J. Adv. Technol. Eng. Sci.* **2014**, *2*, 143–149.
26. Bazhin, V.Y.; Kuskov, V.B.; Kuskova, Y.V. Problems of using unclaimed coal and other carbon-containing materials as energy briquettes. *Ugol* **2019**, *4*, 50–54. [CrossRef]
27. Huang, J.; Li, Z.; Chen, B.; Cui, S.; Lu, Z.; Dai, W.; Zhao, Y.; Duan, C.; Dong, L. Rapid detection of coal ash based on machine learning and X-ray fluorescence. *J. Min. Inst.* **2022**, *256*, 663–676. [CrossRef]
28. Korchevenkov, S.A.; Aleksandrova, T.N. Preparation of Standard Iron Concentrates from Non-Traditional Forms of Raw Material Using a Pulsed Magnetic Field. *Metallurgist* **2017**, *61*, 375–381. [CrossRef]
29. Svoboda, J.; Fujita, T. Recent Developments in Magnetic Methods of Material Separation. *Miner. Eng.* **2003**, *16*, 785–792. [CrossRef]
30. Andronov, G.P.; Zakharova, I.B.; Filimonova, N.M.; L'vov, V.V.; Aleksandrova, T.N. Magnetic Separation of Eudialyte Ore under Pulp Pulsation. *J. Min. Sci.* **2016**, *52*, 1190–1194. [CrossRef]
31. Fokina, S.B.; Petrov, G.V.; Sizyakova, E.V.; Andreev, Y.V.; Kozlovskaya, A.E. Process solutions of zinc-containing waste disposal in steel industry. *Int. J. Civ. Eng. Technol.* **2019**, *10*, 2083–2089.
32. Kairakbaev, A.K.; Abdrakhimov, V.Z.; Abdrakhimova, E.S. The use of ash material of east Kazakhstan in the production of porous aggregate on the basis of liquid-glass compositions. *Ugol'* **2019**, *1*, 70–73. [CrossRef]
33. Lan, M.; He, Z.; Hu, X. Optimization of Iron Recovery from BOF Slag by Oxidation and Magnetic Separation. *Metals* **2022**, *12*, 742. [CrossRef]
34. Petropavlovskaya, V.; Zavadko, M.; Novichenkova, T.; Petropavlovskii, K.; Sulman, M. The Use of Aluminosilicate Ash Microspheres from Waste Ash and Slag Mixtures in Gypsum-Lime Compositions. *Materials* **2023**, *16*, 4213. [CrossRef] [PubMed]
35. Valeev, D.; Kunilova, I.; Alpatov, A.; Varnavskaya, A.; Ju, D. Magnetite and Carbon Extraction from Coal Fly Ash Using Magnetic Separation and Flotation Methods. *Minerals* **2019**, *9*, 320. [CrossRef]
36. Li, W.; Han, Y.; Xu, R.; Gong, E. A Preliminary Investigation into Separating Performance and Magnetic Field Characteristic Analysis Based on a Novel Matrix. *Minerals* **2018**, *8*, 94. [CrossRef]
37. Chen, L.; Xiong, D.; Huang, H. Pulsating High-Gradient Magnetic Separation of Fine Hematite from Tailings. *Min. Metall. Explor.* **2009**, *26*, 163–168. [CrossRef]
38. Luo, L.; Zhang, J.; Yu, Y. Recovering Limonite from Australia Iron Ores by Flocculation-High Intensity Magnetic Separation. *J. Cent. South Univ. Technol.* **2005**, *12*, 682–687. [CrossRef]

39. Wills, B.A.; Napier-Munn, T.J. *Mineral Processing Technology*, 7th ed.; Elsevier Science & Technology Books: Amsterdam, The Netherlands, 2006.
40. Chanturia, V.A.; Minenko, V.G.; Samusev, A.L.; Koporulina, E.V.; Kozhevnikov, G.A. Stimulation of Leaching of Rare Earth Elements from Ash and Slag by Energy Impacts. *J. Min. Sci.* **2022**, *58*, 278–288. [CrossRef]
41. Chen, L.; Qian, Z.; Wen, S.; Huang, S. High-gradient magnetic separation of ultrafine particles with rod matrix. *Miner. Process. Extr. Metall. Rev.* **2013**, *34*, 340–347. [CrossRef]
42. Jin, J.X.; Liu, H.K.; Zeng, R.; Dou, S.X. Developing a HTS Magnet for High Gradient Magnetic Separation Techniques. *Phys. C Supercond.* **2000**, *341–348*, 2611–2612. [CrossRef]
43. Xiong, D.; Liu, S.; Chen, J. New Technology of Pulsating High Gradient Magnetic Separation. *Int. J. Miner. Process.* **1998**, *54*, 111–127. [CrossRef]
44. Bessais, L. Structure and Magnetic Properties of Intermetallic Rare-Earth-Transition-Metal Compounds: A Review. *Materials* **2022**, *15*, 201. [CrossRef] [PubMed]
45. Ding, L.; Chen, L.; Zeng, J. Investigation of Combination of Variable Diameter Rod Elements in Rod Matrix on High Gradient Magnetic Separation Performance. *Adv. Mater. Res.* **2014**, *1030*, 1193–1196. [CrossRef]
46. Song, S.; Lopez-Valdivieso, A.; Ding, Y. Effects of Nonpolar Oil on Hydrophobic Flocculation of Hematite and Rhodochrosite Fines. *Powder Technol.* **1999**, *101*, 73–80. [CrossRef]
47. Su, T.; Chen, T.; Zhang, Y.; Hu, P. Selective Flocculation Enhanced Magnetic Separation of Ultrafine Disseminated Magnetite Ores. *Minerals* **2016**, *6*, 86. [CrossRef]
48. Drozhzhin, V.S.; Shpirt, M.Y.; Danilin, L.D.; Kuvaev, M.D.; Pikulin, I.V.; Potemkin, G.A.; Redyushev, S.A. Formation processes and main properties of hollow aluminosilicate microspheres in fly ash from thermal power stations. *Solid Fuel Chem.* **2008**, *42*, 107–119. [CrossRef]
49. Xiong, T.; Ren, X.; Xie, M.; Rao, Y.; Peng, Y.; Chen, L. Recovery of Ultra-Fine Tungsten and Tin from Slimes Using Large-Scale SLon-2400 Centrifugal Separator. *Minerals* **2020**, *10*, 694. [CrossRef]